ADVANCED FUNCTIONAL MATERIALS
www.afm-journal.de

Single-Step Electrochemical Battery Recycling

*Jarom G. Sederholm, Arghya Patra, Zheng Liu, Jr-Wen Lin, Carlos Juarez-Yescas, Pingfeng Wang, and Paul V. Braun**

Sustainable battery production is a major challenge for the future of electrification with the rise in battery production leading to a massive increase in demand for battery cathode materials. Needed are environmentally responsible ways to recycle used cathodes into new cathodes to create a circular economy for batteries. While some battery recycling and recovery techniques for battery components are developed, they can involve costly and environmentally impactful multi-step processes. This work demonstrates for the first time the simultaneous dissolution and electrochemical deposition of Li-ion transition metal oxide cathodes, providing a path to directly fabricate new battery cathodes from old battery cathodes. The $LiCoO_2$ cathodes formed via this recycling process exhibit near-theoretical capacities, are binder and additive-free, and are phase pure. Technoeconomic and life cycle analyses show the simultaneous dissolution and electrochemical deposition process is less costly and environmentally harmful than traditional pyrometallurgical, hydrometallurgical, and direct recycling methods. This method has major potential impacts and advantages on the industrial scale as it creates battery materials in fewer steps at a lower cost and with a lower environmental impact than current battery recycling methods.

1. Introduction

Battery materials are becoming ever more vital to the global energy landscape with cathode materials constituting the most expensive part of battery cells.[1–6] A significant challenge is the political instability and inhumane mining practices surrounding the mining of materials critical to the production of the highest performing cathode materials.[7] Unless economically viable recycling practices are adopted, large-scale production of batteries will also lead to considerable waste comprised of used battery packs.[8] Used battery packs are additionally dangerous with disposed battery packs leading to fires in waste facilities.[9] As such, there is a growing potential market for battery recycling with estimates setting the market above 20 billion US Dollars annually by 2030.[10,11] Effective recycling efforts will help meet the growing demands for energy materials, reduce waste associated with battery disposal, and enable a sustainable energy storage economy.[12]

Cathode recovery is traditionally performed via hydrometallurgical or pyrometallurgical processes that decompose the lithium transition metal oxide (LTMO) within the cathode into constituent elements or compounds. These processes require multiple steps with various acids, bases, and/or redox controlling agents to remove, separate, and recover each desired recycling product.[8,13–23] The difficulty, cost, and limited overall effectiveness of recovering vital materials from LTMO containing cathodes are all bottlenecks in battery materials recycling[24,25] incentivizing electrification[26] and simplification of recycling processes. There is a body of work on methods for recovering pure LTMOs (as opposed to the constituent elements), including direct recycling processes, to decrease the convolution and cost of battery recycling.[27–32] However, these processes include

J. G. Sederholm, P. V. Braun
Department of Chemical and Biomolecular Engineering, Grainger College of Engineering
University of Illinois Urbana-Champaign
600 S Mathews Ave, Urbana, IL 61801, USA
E-mail: pbraun@illinois.edu

J. G. Sederholm, A. Patra, J.-W. Lin, C. Juarez-Yescas, P. V. Braun
Materials Research Laboratory
University of Illinois Urbana-Champaign
104 S Goodwin Ave MC-230, Urbana, IL 61801, USA

The ORCID identification number(s) for the author(s) of this article can be found under https://doi.org/10.1002/adfm.202511009

DOI: 10.1002/adfm.202511009

J. G. Sederholm, A. Patra, J.-W. Lin, C. Juarez-Yescas, P. V. Braun
Beckman Institute for Advanced Science and Technology
University of Illinois Urbana-Champaign
405 N Mathews Ave, Urbana, IL 61801, USA

A. Patra, J.-W. Lin, C. Juarez-Yescas, P. V. Braun
Department of Materials Science and Engineering, Grainger College of Engineering
University of Illinois Urbana-Champaign
1304 W Green St, Urbana, IL 61801, USA

Z. Liu, P. Wang
Department of Industrial and Enterprise Systems Engineering, Grainger College of Engineering
University of Illinois Urbana-Champaign
104 S Mathews Ave, Urbana, IL 61801, USA

C. Juarez-Yescas, P. V. Braun
Department of Chemistry
University of Illinois Urbana-Champaign
Urbana, IL 61801, USA

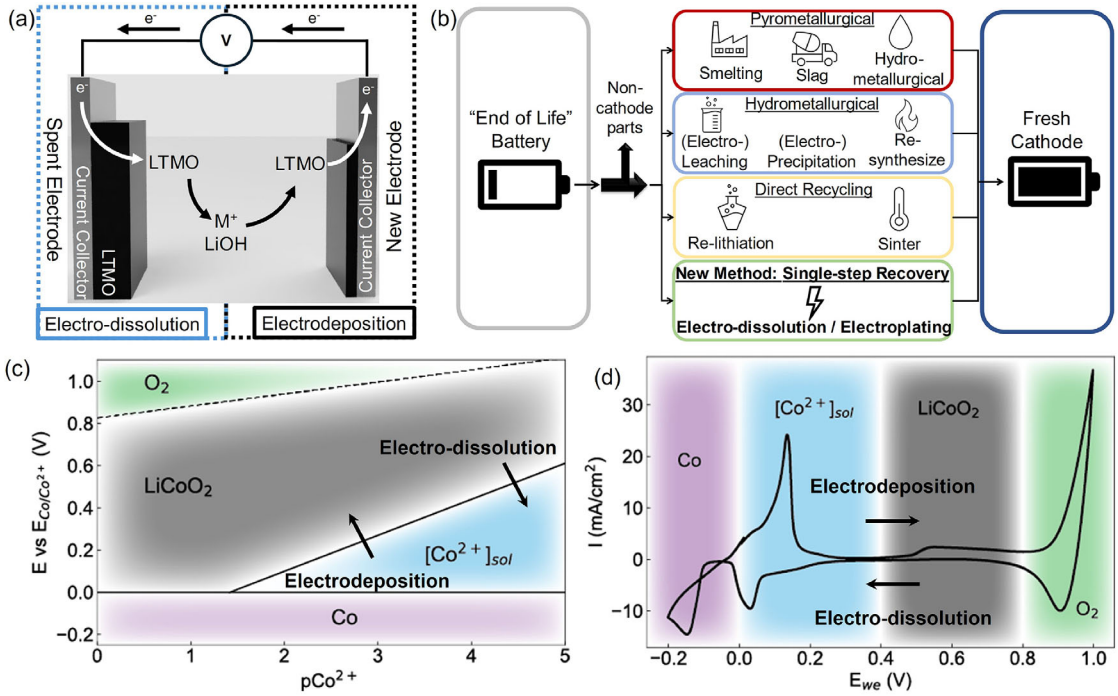

Figure 1. a) A simplified depiction of the single-step electro-dissolution and electrochemical regeneration of lithium transition metal oxide (LTMO) battery cathode materials. b) A simplified comparison between common battery recycling methods (pyrometallurgical, hydrometallurgical, and direct recycling recovery) and our single-step electrochemical recovery. c) Potential-pCo^{2+} diagram depicting the voltage under which the electro-dissolution of LCO will take place as a function of cobalt ion concentration in the molten salt solution. Equations are plotted on a pCo^{2+} scale (-*log*[Co^{2+}]). d) Cyclic voltammetry of a molten salt system at 335°C, 0.01 M of Co^{2+}, and a scan rate of 20 mV s^{-1} with nickel foils serving as both working and counter electrodes and cobalt wire serving as a psuedo reference electrode. Sections are denoted with the electrochemical species most prevalent within the voltages and cobalt ion concentrations shown.

pyrometallurgical and/or hydrometallurgical steps that increase the complexity and cost of the process.[33] The direct recovery methods also struggle to account for morphological changes made to LTMOs during the operating cycle life of the battery causing LTMOs recovered using direct recycling to have poor cycling performance.[34] The problems of battery recycling are only magnified when the environmental and health impacts of the recycling process are considered.[4,35–37] In short, the complexity, cost, and environmental impacts of battery recycling must be significantly reduced to meet the growing need for environmentally responsible battery production and disposal.

Molten salts are of growing interest in battery recycling to meet this need due to their ability to delaminate or dissolve LTMO particles found in a typical cathode, leaving behind the current collectors and other cathode additives, along with molten salt's comparatively low environmental impact.[38,39] However, efforts to recover battery materials using molten salts so far have fallen into similar pitfalls as traditional battery recycling methods in that they still require multiple pre- or post-processing steps.[40–42]

Here, we present a unique single-step process for recovering LTMOs from battery cathodes that leverages molten salt usage while overcoming current battery recycling pitfalls. The single-step process consists of simultaneous molten salt electro-dissolution of old cathodes and electrodeposition of new cathodes that decreases battery recycling complexity, cost, and negative environmental impacts. **Figure 1a** shows a simplified depiction of the process. This process is explored using electrodeposited battery cathodes as both reactant and product. This allows us to explore this process for battery recycling without the addition of cathode additives. Initial experimentation indicates addition of carbon black and PVDF does not impact the single-step process, nor does it lead to impurities in the recovered cathodes. Further experimentation would be required to quantify the impact. The process utilized here produces ultra-dense, battery grade cathode materials. This work focuses on lithium cobalt oxide (LCO) as the LTMO of interest as LCO is a commercial, high performance battery cathode material containing a valuable metal, cobalt. LCO is particularly attractive for this process due to its containing only one transition metal and we already knew how to electrodeposit LCO.[43–45] The metal ion (Co^{2+} in our case) and LiOH shown in the middle of Figure 1a represent the species produced when LCO is electro-dissolved and consumed when LCO is electrodeposited. We note, as methods to electrodeposit other LTMOs emerge, we expect the concept presented in this manuscript will be valuable for recycling of those electrodes too. In this work, the two distinct steps of electro-dissolution and electrodeposition are explored first separately as independent processes. Examples of the electro-dissolution of LCO are provided. Electro-dissolution kinetics are discussed. Evidence of LCO recovery through electrodeposition is provided and the recovered LCO is shown to be phase pure and cycle within a battery cell. The processes are then combined into a single-step to demonstrate growth of new LCO electrodes from old LCO electrodes. Finally, the single-step approach is compared to traditional battery recycling methods and

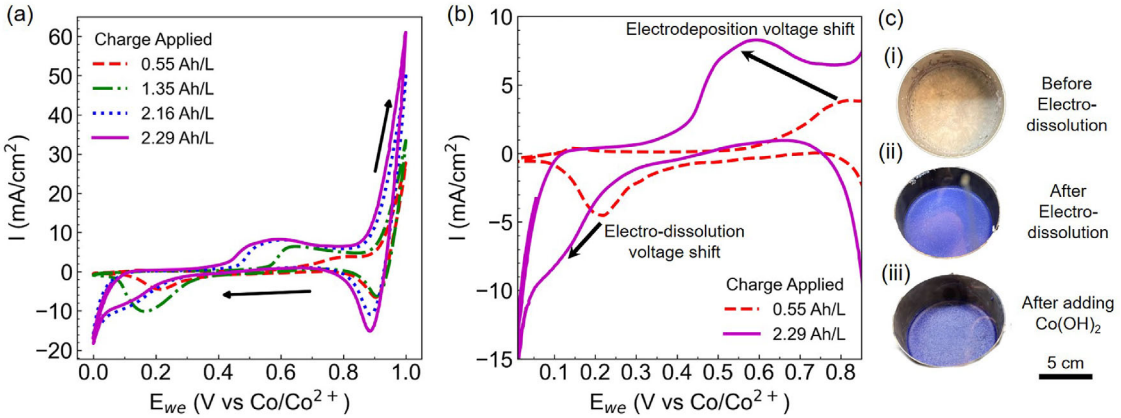

Figure 2. Evidence of cobalt enrichment after increasing levels of electro-dissolution charge (measured in Ah per liter of molten salt bath) are passed in the electro-dissolution molten salt solution. The working and counter electrodes during the cyclic voltammetry are nickel foils and the pseudo reference electrode is a cobalt wire. The temperature of operation is between 300–350°C. Cobalt enrichment is measured by cyclic voltammetry (CV). a) Evolution of the Co^{2+} | Co^{3+} redox peak with passage of increasing charge. The arrows represent the direction of the CVs. b) Portion of CV specific to Co^{2+} | Co^{3+} redox peaks. The arrows indicate the shift in redox peaks of both LCO electrodeposition and LCO electro-dissolution voltage. c) Optical micrographs of the molten salt (regeneration medium) bath i) before electro-dissolution when only LiOH and KOH are present, ii) after electro-dissolution of LCO into the regeneration medium, iii) a bath made similar to the bath of LiOH and KOH but with added $Co(OH)_2$.

is shown to be the least expensive in terms of recycling costs and to have the smallest impact on human health, the ecosystem, and resources. Figure 1b depicts a simplified comparison between the traditional battery recycling methods (pyrometallurgical, hydrometallurgical, and direct recycling) and our single-step battery recovery process.

2. Results and Discussion

The conditions under which the electro-dissolution of LCO within the molten salt takes place is described using a potential-pCo^{2+} diagram (Figure 1c). The lines are produced using the Nernst equation and represent equilibrium lines between different possible electrochemical products. The thermodynamic values and equations used to produce Figure 1c are included in Section SI (Supporting Information). The Co | Co^{2+} transition voltage is used as a psuedo reference voltage and monitored via a cobalt wire. As such, all voltages shown are versus Co | Co^{2+}. [Co^{2+}] in the molten salt solution varies during the electro-dissolution process. It is therefore important to determine the appropriate voltage range to drive LCO dissolution as a function of [Co^{2+}]. Vertical crossings of equilibrium lines in Figure 1c can be observed in cyclic voltammetry (CV) as shown in Figure 1d. The colored boxes shown in Figure 1d correspond to the similarly colored sections in Figure 1c. By operating within the Co^{2+} stable region denoted in Figure 1c,d, electro-dissolution of LCO is the dominant electrochemical reaction. If the process was performed at a voltage lower than the Co^{2+} stable region, conversion of LCO and Co^{2+} to cobalt metal would be the primary electrochemical reaction as shown in the energy dispersive spectroscopy in the Figure S1 (Supporting Information). Operating at voltages higher than the Co^{2+} stable region would electrodeposit LCO rather than electro-dissolve LCO. Even higher voltages would lead to hydroxide decomposition. The CV in Figure 1d does not show other substantive redox peaks nor do we expect a stable Co^{1+} species in the molten salt bath. As such, transitions to and from the Co^{1+} state are not considered in this work.

Electro-dissolution and electrodeposition are investigated as follows. Electro-dissolution is performed using a LCO electrode as the working electrode and a counter electrode capable of oxidation providing the balancing counter electrode reaction. Possible counter electrodes include nickel foils or graphite rods. The nickel foil must be replaced once the surface has been oxidized to the point of passivation and the graphite rods must be replaced when the graphite has been consumed (producing CO_2).

During this process, [Co^{2+}] in the bath increases since no LCO or cobalt is being deposited. Once the bath [Co^{2+}] is sufficient, LCO electrodeposition is possible. To investigate electrodeposition independent of electro-dissolution, the LCO electrode is replaced with a nickel coated stainless steel electrode. LCO is electrodeposited onto this electrode and cobalt metal is electrodeposited on the counter electrode.

Simultaneous electro-dissolution and electrodeposition utilizes a LCO containing electrode and a stainless steel film containing an electrodeposited LCO seed layer or nickel foil as the counter electrode. While a LCO seed layer is not necessary, it improves the conformity of the grown LCO. The concurrent electro-dissolution and electrodeposition LCO recycling and growth process is compared to other LCO producing processes through technoeconomic analysis (TEA) and life cycle impact assessment (LCIA). LCIA is performed using the ReCiPe method and is included with TEA in Section SII (Supporting Information).

2.1. LCO Electro-Dissolution

The increase of cobalt ions in solution from electro-dissolution of LCO is observable through multiple metrics including visually and via CV. **Figure** 2a exhibits CVs taken of a nickel working electrode with a nickel counter electrode and a cobalt wire as a pseudo reference electrode in the molten salt regenerative

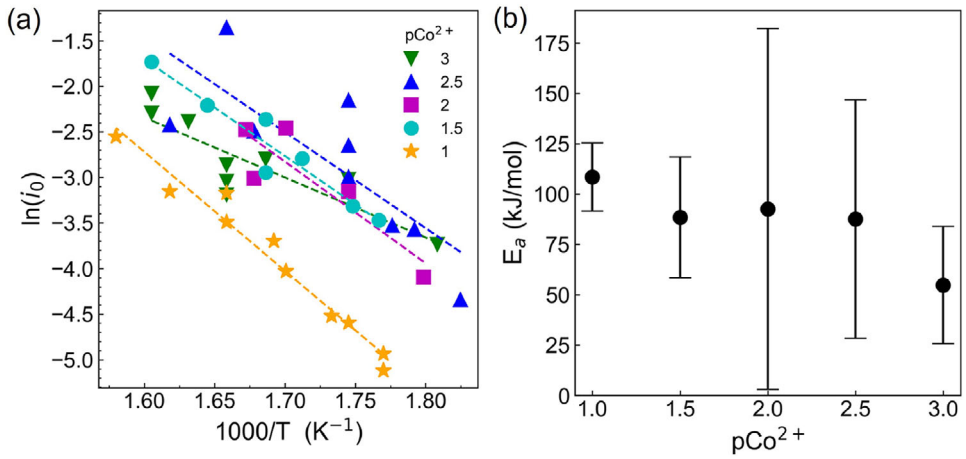

Figure 3. Kinetic analysis of electro-dissolution. a) Arrhenius style plot of the exchange current density (i_0) at 5 $[Co^{2+}]$ (10^{-3} M, $10^{-2.5}$ M, 10^{-2} M, $10^{-1.5}$ M, 0.1 M). Activation energies, 95% confidence intervals, and coefficient of determination, R^2, values gathered from data fitting are included in Table S1 (Supporting Information). b) Activation energies as a function of $[Co^{2+}]$ with 95% confidence intervals.

solution after increasing amounts of electro-dissolution charge have been applied. The location of the redox peaks correlated with the Co^{2+} | Co^{3+} transition should decrease as the $[Co^{2+}]$ in the regenerative solution increases as shown in Figure 1c. This is observed experimentally as the Co^{2+} | Co^{3+} peaks, denoted as 'electrodeposition voltage' and 'electro-dissolution voltage' in Figure 2b, shift to the left as the amount of electro-dissolution charge passed increases. All other conditions through electro-dissolution are the same except for a negligible increase in LiOH. Further evidence of electro-dissolution of LCO into the molten salt bath can be observed visually. Before electro-dissolution, the molten salt is a nearly colorless liquid (Figure 2 ci). After LCO electro-dissolution, the molten salt bath is deep blue (Figure 2 cii). The bath in Figure 2 cii is visually similar to Figure 2 ciii, a molten salt bath containing added $Co(OH)_2$. Another visual example is found in Figure S2 (Supporting Information) which shows the electrodeposited LCO electrodes at increasing stages of electro-dissolution with the sample in the upper left corner being a LCO sample that has been completely electro-dissolved and samples to the right and then down showing decreasing degrees of electro-dissolution. XRDs of the nickel counter electrodes used during this process are provided in Figure S3 (Supporting Information). The XRDs confirm that the only product formed on the nickel counter electrode surface is nickel oxide. These XRD patterns indicate that NiO does not dissolve well into the bath. Addition of nickel hydroxide to the bath produces a nickel precipitate in the bath as well. As such, Ni^{2+} introduction into the bath is considered to be minimal to none. The electro-dissolution process is stopped at the desired $[Co^{2+}]$. This may require multiple nickel counter electrodes. Figure S4 (Supporting Information) shows how passivation of the nickel counter electrode is indicated by an observable rise in the counter electrode voltage. At this point, the nickel counter electrode must be replaced to continue LCO electro-dissolution. An optical micrograph of the Ni counter electrodes are shown in Figure S5 (Supporting Information).

The kinetics of LCO electro-dissolution is investigated assuming Equation (1) is the reaction of interest. This reaction is evaluated using the Butler-Volmer equation shown in Equation (2).[46] Note, the interface for a molten salt varies from that of traditional organic and aqueous systems. Therefore, the application of Butler-Volmer serves only as an approximation for determining electrokinetic parameters of this molten salt system.

$$LiCoO_2 + H_2O + e^- \underset{\text{Electrodeposition}}{\overset{\text{Electro-dissolution}}{\rightleftharpoons}} CoO + LiOH + OH^- \quad (1)$$

$$i = i_0[e^{-\alpha f \eta} - e^{(1-\alpha) f \eta}] \quad (2)$$

$$i_0(T) = Ae^{\frac{-E_a}{RT}} \quad (3)$$

Operating voltages near the open circuit voltage are utilized to ensure the mass transfer effects were avoided as required for Butler-Volmer kinetics. The current responses from each of the voltages are gathered and then fit to the Butler-Volmer equation to solve for the exchange current density, i_0, and the transfer coefficient, α, with f representing Faraday's constant divided by the product of the gas constant and temperature. i_0 has an Arrhenius dependence on temperature (Equation (3)[47]) and by fitting i_0 values to an Arrhenius equation as shown in **Figure 3**a, we determine the activation energy (E_a) at five $[Co^{2+}]$ from 10^{-3} M to 0.1M. The activation energy obtained from fitting the data to the Arrhenius equation is shown in Figure 3b. The error bars attached to the activation energy values represent 95% confidence intervals of the activation energy based off the regression used to fit the i_0 data to the Arrhenius equation. The activation energy, 95% confidence intervals, and coefficients of regression are included in Table S1 (Supporting Information). These graphs show that activation energy of this process is likely concentration independent over a large $[Co^{2+}]$ range and appears to be around 90-100 kJ mol^{-1}. The most commonly obtained value of α from the

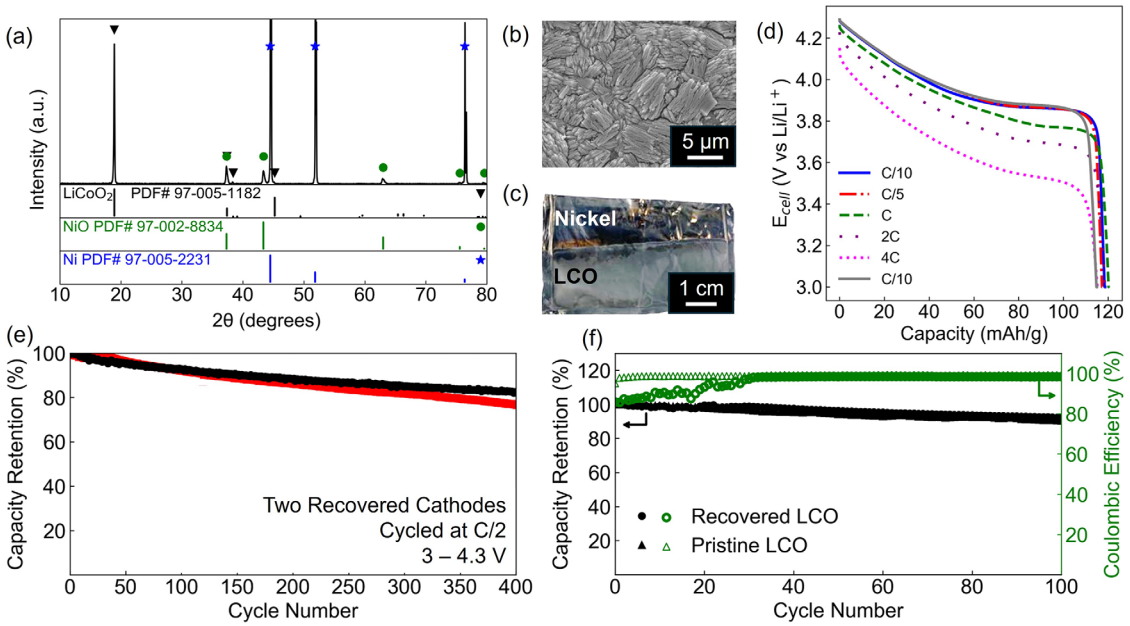

Figure 4. a) X-ray diffraction (XRD) of a LCO electrode electrodeposited from the solution used for electro-dissolution. The change in peak intensities relative to the standard LCO signal is a result of the crystallographic texturing of the LCO. b) Scanning electron micrograph of the surface of a LCO electrode electrodeposited from the electro-dissolution molten salt solution. c) Picture of a LCO cathode made from electrodeposition in the molten salt bath. d) Discharge profiles of a LCO electrode produced from the electro-dissolution molten salt bath versus lithium (4.59 mg cm^{-2}). Cells were cycled in the order C/10, C/5, C, 2C, 4C, and C/10. All cycles were charged at a rate of C/10. e) Extended cycling of two cells produced using material recovered through electrodeposition cycled at C/2 from 3.0 to 4.3V versus lithium. f) Capacity retention and coulombic efficiency of batteries produced from the materials recovered through electrodeposition and pristine materials over 100 charging/discharging cycles at a rate of C/2. Pristine electrodes were cycled from 3 to 4.2 V and electrodes recovered through electrodeposition were cycled from 3 to 4.3 V.

fitting is at or near unity. These results demonstrate that electro-dissolution current remains largely unaffected by [Co^{2+}] over several decades of concentration before decreasing at higher [Co^{2+}].

2.2. LCO Electrodeposition

Once the [Co^{2+}] is sufficient, the same molten salt bath used for electrodissolution can be used for electrodeposition of LCO cathodes following the general approach we have published previously.[43–45] XRD (**Figure 4**a) confirms the deposit is LCO (note, during this process, cobalt metal is deposited on the counter electrode). The LCO crystals are oriented causing a difference between the sample XRD peak intensities and the standard peak intensity of LCO. The highly crystalline <110 > facet of LCO is observable under SEM (Figure 4b). Note, this is not the same sample as shown in the XRD. An optical micrograph of a LCO electrode produced during these experiments is shown in Figure 4c. The electrodeposited LCO is annealed at 600 °C for four hours and used as the cathode in a coin cell with lithium foil anodes. The cell formed using LCO recovered through electrodeposition is tested to determine its discharge rate performance (Figure 4d). The rate test shows that the LCO recovered has favorable electrochemical performance as it maintains its capacity despite being charged at rates as high as 4C. The cyclability of the recovered LCO cell is also favorable. Figure 4e shows the two cells containing LCO recovered through electrodeposition cycle hundreds of times before reaching 80% capacity retention at a charge/discharge rate of C/2 from 3.0V to 4.3V versus lithium, with one cell retaining 80% capacity retention for 500 cycles. Figure 4f shows the coulombic efficiency and the capacity retention over 100 cycles for cells containing cathodes made from recovered LCO and pristine LCO. The recovered LCO performs similarly to the pristine material in terms of both capacity retention and cyclability. Pristine materials have been shown to have high performance in full cells at high discharging rates in our previous work.[43–45] Based on the similarities of the recovered material to the pristine material, with optimization (outside the scope of this study) we expect the recovered materials will perform comparably. The recovered LCO shows an initial drop in efficiency and we suspect the initial drop is due to the recovered material being over-lithiated during electrodeposition. Over the first few cycles, the excess lithium in the recovered LCO transfers to the lithium anode. This explains why the coulombic efficiency is below 100% without impacting the capacity retention.

2.3. Simultaneous LCO Electro-Dissolution and Electrodeposition

In what is the most attractive mode of operation, electro-dissolution and electrodeposition are combined. We refer to this as the single-step method. Unlike when the LCO dissolution and deposition steps are separate, this approach productively balances reactions at both electrodes and thus neither requires a sacrificial counter electrode (required for the LCO dissolution-only method) nor results in cobalt metal plating on the counter

electrode (LCO deposition only method). The single-step process can be performed as shown in Figure 1a in two variants, both of which electro-dissolve and electrodeposit LCO. When the LCO stripping electrode is the working electrode, we refer to the process as cathodic single-step recovery, and when the LCO deposition electrode is the working electrode we refer to the process as anodic single-step recovery. The difference is to which electrode the reference electrode voltage is associated with. In anodic single-step recovery, one has more control over the deposition of LCO. This allows for more control of the crystallographic orientation of LCO during plating[43–45] to produce high performance additive-free battery cathodes. Cathodic single-step recovery focuses on the electro-dissolution of LCO with less control over the orientation of LCO that is plated. Cathodic recovery is more applicable to processes where the LCO would be removed from the counter electrode, further processed, and provided as a powder. Cathodic single-step recovery also requires lower voltages. For successful LCO growth in cathodic single-step recovery, the counter electrode (typically Ni) needs to be passivated such that the electrode voltage rises to potentials where LCO growth is favorable. The simplest way to passivate the counter electrode surface is to electrodeposit a thin layer of LCO on it via our standard LCO electrodeposition approach before placing it in the single-step bath so that the counter electrode voltage lies within the voltage range where LCO is stable as shown in Figure 1c.

XRD collected from an electrode made through anodic single-step recovery is shown in **Figure 5a**. The XRD confirms the growth of LCO using the single-step method. An XRD spectra of a nickel counter electrode that was used as a counter electrode during the electro-dissolution experiments ('Electro-dissolution Only' spectra) is included as a reference. XRDs of multiple LCO-coated electrodes formed via cathodic single-step recovery are provided in Figure S6 (Supporting Information). The faradaic efficiency (FE) of the anodic single-step process is dependent on $[Co^{2+}]$ as shown in Figure 5b. The FE of the anodic single-step recovery process is evaluated by measuring the amount of LCO electrodeposited or the amount of LCO electro-dissolved in comparison to charge that was passed. For these experiments, electrodeposited LCO is used as both the working and the counter electrode. Before measuring the final sample mass, the sample is washed with water to remove residual molten salt and then dried to remove water. The FE of electrodeposition is low when $[Co^{2+}]$ is small and increases with increasing $[Co^{2+}]$. The negative numbers at low $[Co^{2+}]$ are most likely due to gas generation removing LCO (when $[Co^{2+}]$ is zero, the only reaction is oxidation of the hydroxide into O_2). This matches the results seen in Figure 1d where solvent consumption peaks are observed at oxidative potentials. Figure 1c also shows that oxygen evolution through hydroxide degradation would be expected at higher positive voltages. This gas formation may have caused removal of pieces of LCO. FE of LCO electrodeposition then increases as $[Co^{2+}]$ increases. Note, a possible loss of efficiency for electrodeposition throughout the experiments is that some of the LCO formed may precipitate rather than adhere to the electrode or LCO may also be removed during the washing of the electrode. The FE of electro-dissolution is near 80% and above for most experiments. In cases where the FE of LCO dissolution is above 100%, we suspect some LCO is lost during washing. The totality of the results indicates the anodic single-step process is most advantageous above 10^{-2} M Co^{2+} where the FE of electro-dissolution and electrodeposition are both near or above 80%. LCO produced from anodic single-step recovery was then annealed at 600 °C for four hours and evaluated by using the LCO as a cathode in a coin cell with a lithium metal anode. Figure 5c shows the electrochemical properties of this single-step cathode in comparison to coin cells produced using pristine LCO and LCO formed via electro-dissolution followed by electrodeposition (referred to as 'Recovered', this is the same cathode made during the electrodeposition section of this work) for 50 cycles. The materials recovered through single-step perform similarly in capacity retention to pristine materials and the materials recovered earlier in this work. This indicates the cathodes produced from this method may perform as well as the high rate capable and stable pristine materials, although further material optimization may be required.

We further explored the stability of the molten salt after extended single-step recovery processes. In order to do so, we first applied 10 s on 30 s off current pulses near 1 mA cm^{-2} to a LCO working electrode (with LCO also used as the counter electrode) at a bath chemistry of near 0.1M Co^{2+}. After an hour, the current was changed to near -1 mA cm^{-2}. In doing so, we ensure that neither electrode runs out of LCO to be electro-dissolved. If the working electrode voltage decreases below 0V, the electrodes are replaced as this indicates delamination or complete loss of LCO. The process was run for roughly 60 h with temperature being maintained between 300 and 340°C. The working and counter electrode voltages for the 60 h is shown in Figure 5d. The decrease in the working and counter electrode voltages after replacing the electrodes a second time is likely caused by slightly different LCO electrodes being used as the working and counter electrodes. After the completion of the stability experiment, we introduced a new LCO working and counter LCO electrode and ran the single-step recovery process. The FEs for the electrodeposition and electro-dissolution processes were 89.9% and 71.9%, respectively. This indicates that the single-step process can be run for long periods of time without replacing the molten salt medium and maintain a desirable FE. This simplifies and decreases the cost of recovering the battery material. An illustration of the single-step process is shown in Figure 5e. The process is further detailed in Figure S7 (Supporting Information) to include an electro-dissolution only section for enriching the bath before single-step recovery.

2.4. Techno-Economic Analysis and Life Cycle Impact Assessment

To evaluate the feasibility of implementation, the cathodic single-step recovery of unannealed LCO is compared to pyrometallurgical, hydrometallurgical, and direct recycling processes along with mining and refining new materials through the lens of both a TEA and a LCIA. We adopted continuous stirred tank reactors and ovens for all processes to standardize the process for fair comparison. The reactor has a capacity of 10,000 kg with the later processes and equipment accommodated to fit the capacity of the 10,000 kg reactor. Pyrometallurgical (modeled as a combination of a high temperature calcination step followed by a hydrometallurgy step),[48] hydrometallurgical,[49] direct,[50] and mining methods[51] were modeled using processes

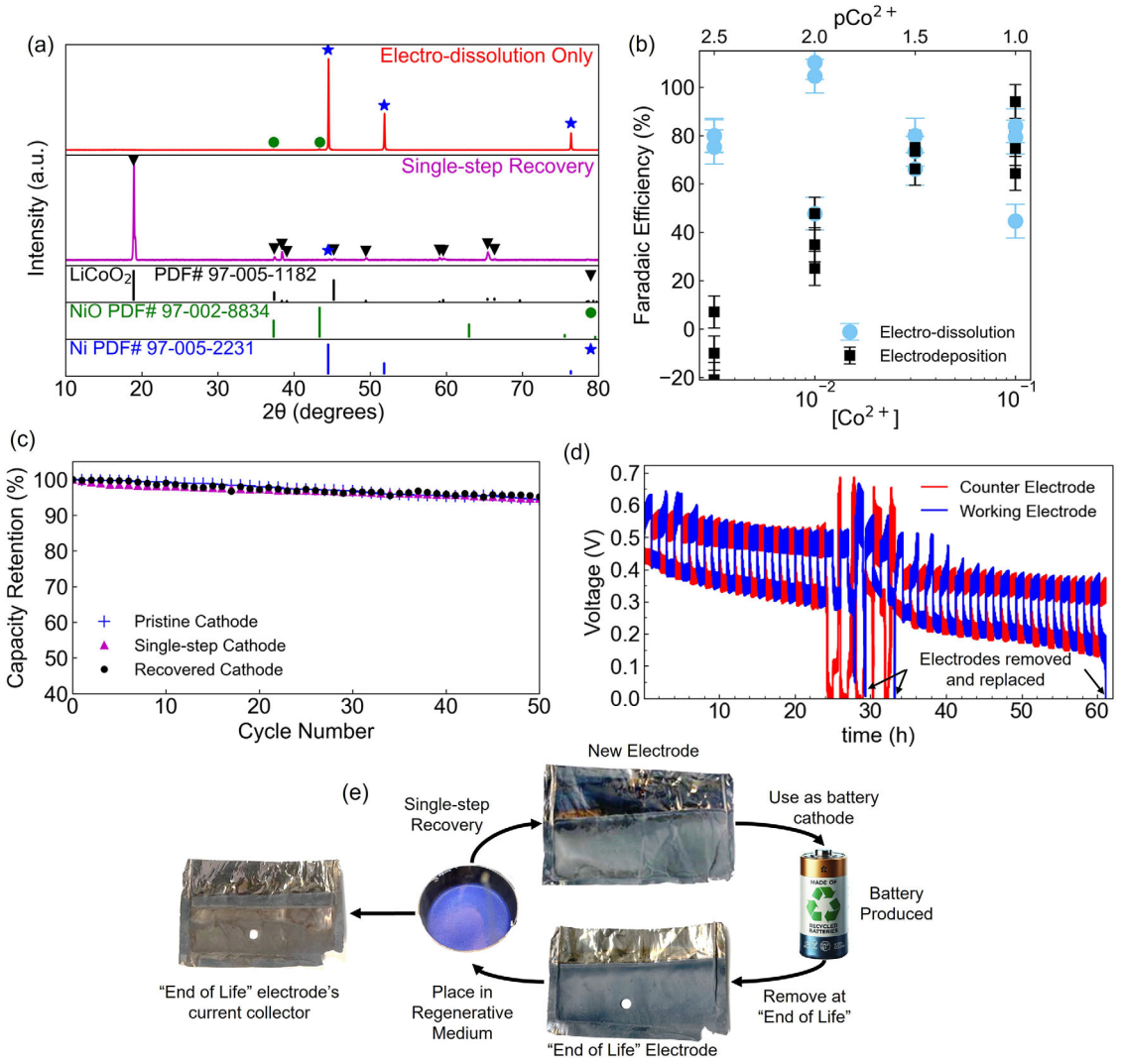

Figure 5. a) XRD comparison of nickel foil electrodes during electro-dissolution only and anodic single-step processes. The single-step recovery electrode shows LCO peaks while the electro-dissolution foil has no such signals. Included are reference spectra for nickel, nickel oxide, and $LiCoO_2$. b) Faradaic efficiency of electrodeposition and electro-dissolution during cathodic single-step recovery process at different $[Co^{2+}]$. Each data point represents a single-step recovery experiment. Bars represent measurement uncertainties. c) Cycle life comparison of cells produced using cathodes produced by electrodeposition from pristine materials (pristine cathode), anodic simultaneous electro-dissolution and electrodeposition (single-step cathode), and electrodeposition of electro-dissolved materials (recovered cathode). All cycled at a rate of C/2. The pristine electrode was cycled from 3 to 4.2V while multi-step and single-step electrodes were cycled from 3 to 4.3V. d) LCO working and counter electrode voltages during long-term electrolyte stability test. Positive and negative current pulses of 10 s on, 30 s off were applied at a current density near 1 mA cm^{-2}. When the working electrode voltage decreased below 0V, the LCO working and counter electrodes were removed and replaced. e) Depiction of the full single-step recovery process from "End-of-Life" LCO electrodes to a continuous cycle of recovering and producing new LCO electrodes (battery image produced by AI).

in other published works. Single-step was scaled up assuming a linear volumetric dependence rather than surface area dependence as electrodes are suspended in solution rather than reacting with the walls of the reactor. Both TEA and LCIA values of the single-step process assume a daily change of molten salt regenerative medium. Dismantling, transportation, and impurity removal processes, which are required for all recycling processes are not included including binder and carbon black separation. All processes begin as if only the cathode active material is being processed. All processes end with new LCO produced. TEA assesses the processes in terms of cost per kilogram of LCO produced. The costs used in this analysis include equipment depreciation, equipment maintenance, energy, water, labor, and input material costs. The evaluation of each of these costs is included in Section SII (Supporting Information) along with the input costs required for each process with a corresponding source and the individual calculated values of each cost for all recycling/production methods. As illustrated in **Figure 6a**, the cost of the single-step method is much lower than other methods. To understand why the single-step method has a lower cost, the TEA for the single-step and direct recycling methods are split into their constituent costs (Figure 6b). In Figure 6b,

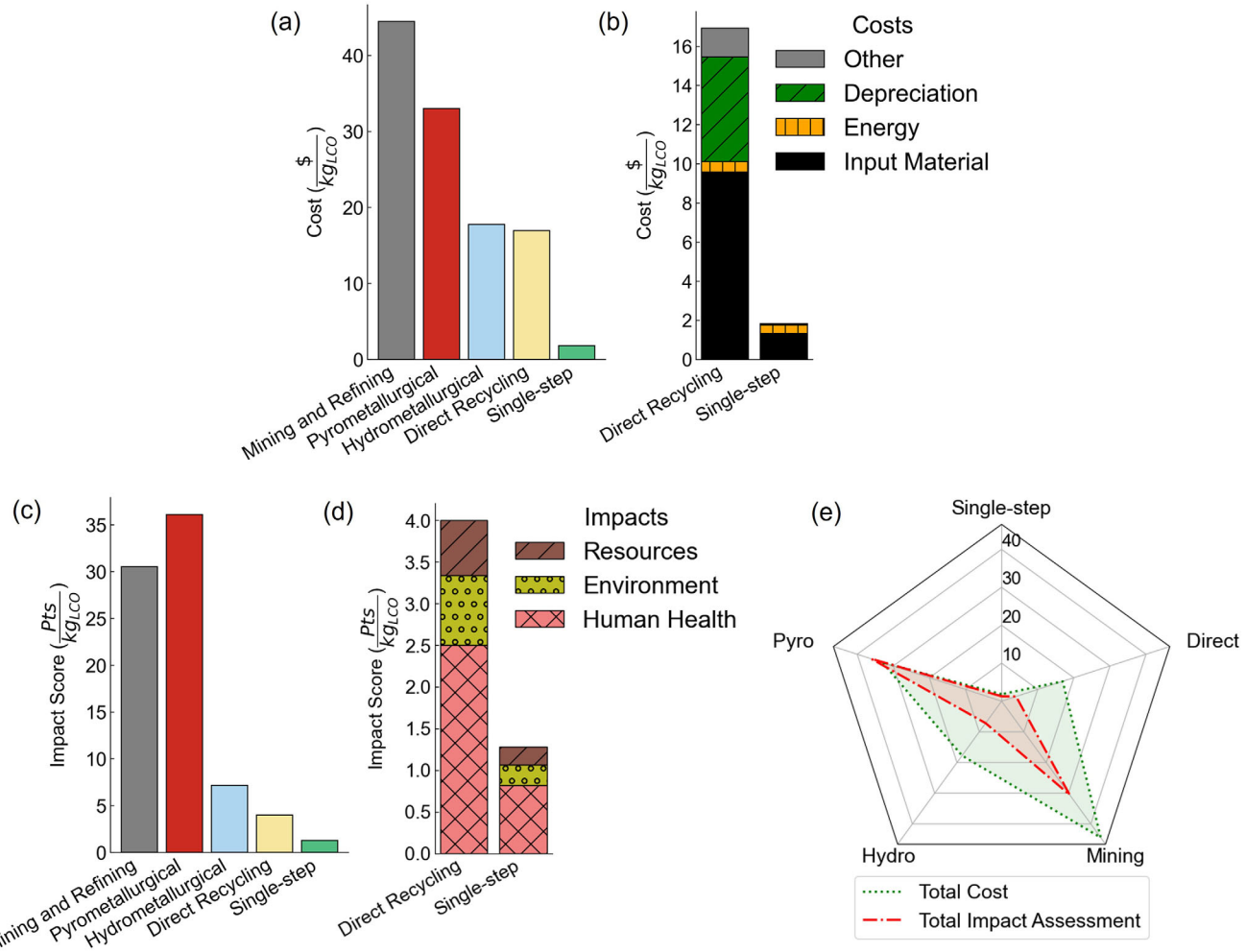

Figure 6. Techno-economic analysis (TEA) and life cycle impact assessment (LCIA) normalized in units per kg of LCO produced. a) A TEA comparison of LCO recycling/production methods. b) A TEA comparison of direct recycling and the single-step method split into costs. c) A LCIA comparison of LCO recycling/production methods. d) A LCIA comparison of direct recycling and the single-step method with impacts scores split into impacts. e) A radar plot comparing LCO recycling/production methods in terms of both total cost and total impact assessment per kg LCO.

the costs are only split up into input material cost, energy cost, depreciation cost, and a summation of all other costs (other, includes cost of maintenance, water, and labor). Figure 6b shows that the cost is kept low in the proposed single-step recovery by reusing the same medium as much as possible to decrease input material costs while also using less energy. The larger depreciation cost in direct recycling is due to the cost of using high-temperature ovens for sintering regularly.

The single-step method continues to be superior to other LCO production processes in terms of LCIA. The LCIA of each process is evaluated using the ReCiPe model[52] which includes impact categories such as particulate matter production, global warming, freshwater ecotoxicity, and mineral resource usage. Each of these categories is then grouped into impact on global resources, human health, or the ecosystem. The total impact factor is calculated by summing each of these factors together. This means a small impact factor is preferable. A description of the analysis is included in Section SII (Supporting Information). Figure 6c shows that the single-step method has a smaller impact than any other LCO production method. Similar to the TEA, the total LCIA of direct recycling and single-step recovery are separated into individual impact factors and shown in Figure 6d. The figure shows that the single-step method has a markedly smaller impact in all categories meaning that the single-step method is a safer process to humanity, less harmful to the ecosystem, and more resource sustainable. This is vital as we move forward as a more conscience energy community. Figure 6e is included to show how each LCO production method compares in both total impact and cost with a lower value being advantageous in both TEA and LCIA.

Both TEA and LCIA results are supplemented with results gathered using the EverBatt module created by Argonne National Lab.[53] The EverBatt module considers battery transportation, recycling of the entire battery cell, and more industrial process steps than included in the analyses above. However, the EverBatt model used to define the single-step process uses shredding techniques common to industry that would not be conducive to the method shown here. As such, the results are used only as a

supplement to the data gathered in Figure 6. The results of the TEA and LCIA are included in Figures S8 and S9 (Supporting Information). The results show again that the single-step process is cheaper and less environmentally impactful than direct recycling processes assuming a monthly replacement of molten salt media.

3. Conclusion

In summary, this work presents a novel single-step method for recovering the LTMO LCO, a critical energy storage material, via a combined molten salt electro-dissolution and electrodeposition process. LCO cathodes made via the approach presented here have rate capability and cyclability similar to those electrodeposited from pristine materials. This recovery process can improve the current battery recycling industry and is superior to the current battery recycling methods in terms of recycling costs and total impact on human health, the ecosystem, and global resources. We suggest that the application of this method at an industrial scale would be economical and environmentally friendly. This work demonstrates the impact single-step recovery can have on LCO recovery. As methods to electrodeposit other LTMOs are developed, we believe the approach described here will also be applicable for recycling of those chemistries as electrodeposition of high-quality electrodes is more challenging than electrodissolution. Further development of methods to electrodeposit other LTMOs likely will enable the single-step recovery of those same electrodes.

4. Experimental Section

All processes were performed using a three electrode setup utilizing a cobalt wire pseudo reference electrode. The electrodes were dipped in a near eutectic molten salt solution of lithium and potassium hydroxide. By utilizing a eutectic mixture, the salt melting temperature was decreased, decreasing the energy requirements of the process. The reaction vessel consisted of an Inconel crucible and quartz or borosilicate lid capable of withstanding higher temperatures and highly alkaline environments. The three electrodes were attached to the lid such that all three electrodes were sufficiently immersed in the molten salt. The solution was dried under vacuum and mixed to provide homogeneous conditions for the electrodissolution and electrodeposition processes. Note, maintaining a low concentration of water within the molten salt solution was important. The electrochemical processing was performed under nitrogen gas. Coin cells were constructed from stainless steel coin cell casings (MTI corporation), a commercial electrolyte (RD810, Gotion Inc.), and an appropriate separator (Celgard,Whatman).

X-ray diffraction data was taken at steps of 0.01 degrees from 10° to 80° using a copper $K\alpha_1$ source.

In the technoeconomic analysis, the electricity price, water price, and labor wages were considered to be \$0.1181/kWh, \$0.89/ton, and \$32 per hour, respectively.

Statistical Analysis: For the kinetic analysis, the same electrodeposited LCO was used for each test until the LCO was removed. The LCO was then replaced with a new electrodeposited LCO. It was validated that each electrodeposited LCO produced similar kinetic results. The 95% confidence intervals were calculated as follows. The standard error was calculated by taking the square root of the covariance found when fitting the Arrhenius equation to the gathered data. The degrees of freedom were determined by the number of samples (N) subtracted by the number of parameters (P) determined from the fitting which was two for the study (the activation energy and the pre-exponential factor). The number of samples for the 10^{-3}, $10^{-2.5}$, 10^{-2}, $10^{-1.5}$, and 0.1 M were 9, 9, 5, 7, and 10, respectively.

For the faradaic efficiency experiments, applied voltages changed for each $[Co^{2+}]$. The voltages used were 0.7, 0.85, 0.6, and 0.6V for pCo^{2+} of 2.5, 2, 1.5, and 1, respectively. The error bars represent the uncertainty stemming from the measurement of the mass of the sample.

Supporting Information

Supporting Information is available from the Wiley Online Library or from the author.

Acknowledgements

The authors acknowledged Prof. Theresa Schoetz and Prof. Joaquín Rodríguez-López for helpful discussion. Work at the University of Illinois Urbana-Champaign was supported by the National Science Foundation Future Manufacturing Research Grant under award CMMI-2037898. Aspects of this work were carried out in the University of Illinois Materials Research Laboratory Central Facilities. [Correction added on October 27, 2025, after first online publication: Textual eroor has been corrected.]

Conflict of Interest

Jarom G. Sederholm, Arghya Patra, and Paul V. Braun have an application for a patent related to this work (International Patent Application No. PCT/US2023/34518 based on US 63/414,956).

Data Availability Statement

The data that support the findings of this study are available in the supplementary material of this article.

Keywords

battery recycling, cathodes, li-ion battery, sustainable battery production

Received: June 12, 2025
Revised: July 2, 2025
Published online:

[1] D. Thompson, C. Hyde, J. M. Hartley, A. P. Abbott, P. A. Anderson, G. D. J. Harper, *Resources, Conservation and Recycling* **2021**, *175*, 105741.
[2] A. Zeng, W. Chen, K. D. Rasmussen, X. Zhu, M. Lundhaug, D. B. Müller, J. Tan, J. K. Keiding, L. Liu, T. Dai, A. Wang, G. Liu, *Nature Communications* **2022**, *13*, 1341.
[3] C. Xu, Q. Dai, L. Gaines, M. Hu, A. Tukker, B. Steubing, Future material demand for automotive lithium-based batteries, *Communications Materials* **2020**, *1*, 99.
[4] M. Chen, X. Ma, B. Chen, R. Arsenault, P. Karlson, N. Simon, Y. Wang, *Joule* **2019**, *3*, 11.
[5] H. Hao, Y. Geng, J. E. Tate, F. Liu, K. Chen, X. Sun, Z. Liu, F. Zhao, *Nature Communications* **2019**, *10*, 5398.
[6] J. Baars, T. Domenech, R. Bleischwitz, H. E. Melin, O. Heidrich, *Nature Sustainability* **2021**, *4*, 71.
[7] M. Davie, https://www.abc.net.au/news/2022-02-24/cobalt-mining-in-the-congo-green-energy/100802588, (accessed: March 2025).
[8] G. Harper, R. Sommerville, E. Kendrick, L. Driscoll, P. Slater, R. Stolkin, A. Walton, P. Christensen, O. Heidrich, S. Lambert, A. Abbott, K. Ryder, L. Gaines, P. Anderson, *Nature* **2019**, *575*, 75.

[9] L. Kong, C. Li, J. Jiang, M. G. Pecht, *Energies* **2018**, *11*, 9.
[10] S. Kumawat, D. Singh, A. Saini, *Materials and Manufacturing Processes* **2023**, *38*, 2.
[11] N. Kachate, D. Sharma, K. Baidya, *Materials Today: Proceedings* **2023**, *72*, 1498.
[12] J. G. Sederholm, L. Li, Z. Liu, K.-W. Lan, E.-J. Cho, Y. Gurumukhi, M. J. Dipto, A. Ahmari, J. Yu, M. Haynes, N. Miljkovic, N. H. Perry, P. Wang, P. V. Braun, M. C. Hatzell, *ACS Energy Letters* **2024**, *10*, 1.
[13] K. Kim, D. Raymond, R. Candeago, X. Su, *Nature Communications* **2021**, *12*, 6554.
[14] W. Lv, Z. Wang, H. Cao, Y. Sun, Y. Zhang, Z. Sun, A Critical Review and Analysis on the Recycling of Spent Lithium-ion Batteries, *ACS Sustainable Chemistry and Engineering* **2018**, *6*, 2.
[15] D. A. Ferreira, L. M. Z. Prados, D. Majuste, M. B. Mansur, *Journal of Power Sources* **2009**, *187*, 1.
[16] M. K. Tran, M. T. F. Rodrigues, K. Kato, G. Babu, P. M. Ajayan, *Nature Energy* **2019**, *4*, 339.
[17] J. Piatek, T. M. Budnyak, S. Monti, G. Barcaro, R. Gueret, E. S. Grape, A. Jaworski, A. K. Inge, B. V. M. Rodrigues, A. Slabon, *ACS Sustainable Chemistry and Engineering* **2021**, *9*, 29.
[18] N. Schaeffer, H. Passos, M. Gras, S. J. R. Vargas, M. C. Neves, L. Svecova, N. Papaiconomou, J. A. P. Coutinho, *ACS Sustainable Chemistry and Engineering* **2020**, *8*, 32.
[19] Z. Liang, C. Cai, G. Peng, J. Hu, H. Hou, B. Liu, S. Liang, K. Xiao, S. Yuan, J. Yang, *ACS Sustainable Chemistry and Engineering* **2021**, *9*, 17.
[20] M. Assefi, S. Maroufi, Y. Yamauchi, V. Sahajwalla, *ACS Sustainable Chemistry and Engineering* **2019**, *7*, 23.
[21] F. Zhou, X. Qu, Y. Wu, J. Zhao, S. Gao, D. Wang, H. Yin, *ACS Sustainable Chemistry and Engineering* **2022**, *10*, 3.
[22] J. Zhang, J. Hu, Y. Liu, Q. Jing, C. Yang, Y. Chen, C. Wang, *ACS Sustainable Chemistry and Engineering* **2019**, *7*, 6.
[23] L. Li, R. Chen, F. Sun, F. Wu, J. Liu, *Hydrometallurgy* **2011**, *108*, 3.
[24] Z. J. Baum, R. E. Bird, X. Yu, J. Ma, *ACS Energy Letters* **2022**, *7*, 2.
[25] M. Kaya, *Circular Economy* **2022**, *1*, 2.
[26] W. Wang, Z. Liu, Z. Zhu, Y. Ma, K. Zhang, Y. Meng, T. Ahmad, N. A. Khan, Q. Peng, Z. Xie, Z. Zhang, W. Chen, *Nature Sustainability* **2025**, *8*, 287.
[27] R. Zhan, Z. Oldenburg, L. Pan, *Sustainable Materials and Technologies* **2018**, *17*, e00062.
[28] The ReCell Center for Advanced Battery Recycling - FY22 Q1 Report. Technical Report, Argonne National Laboratory, **2022**.
[29] Z. Zheng, M. Chen, Q. Wang, Y. Zhang, X. Ma, C. Shen, D. Xu, J. Liu, Y. Liu, P. Gionet, I. O'Connor, L. Pinnell, J. Wang, E. Gratz, R. Arsenault, Y. Wang, *ACS Sustainable Chemistry and Engineering* **2018**, *6*, 11.
[30] K. Park, J. Yu, J. Coyle, Q. Dai, S. Frisco, M. Zhou, A. Burrell, *ACS Sustainable Chemistry and Engineering* **2021**, *9*, 24.
[31] Y. Bai, R. Essehli, C. J. Jafta, K. M. Livingston, I. Belharouak, *ACS Sustainable Chemistry and Engineering* **2021**, *9*, 17.
[32] K. Jia, J. Ma, J. Wang, Z. Liang, G. Ji, Z. Piao, R. Gao, Y. Zhu, Z. Zhuang, G. Zhou, H.-M. Cheng, *Advanced Materials* **2022**, *35*, 5.
[33] X. Yu, W. Li, V. Gupta, H. Gao, D. Tran, S. Sarwar, Z. Chen, *Global Challenges* **2022**, *6*, 12.
[34] L. Gaines, *Sustainable Materials and Technologies* **2018**, *17*, e00068.
[35] R. E. Ciez, J. F. Whitacre, *Nature Sustainability* **2019**, *2*, 148.
[36] L. Gaines, *One Earth* **2019**, *1*, 4.
[37] B. J. Ross, M. Leresche, D. Liu, J. L. Durham, E. U. Dahl, A. L. Lipson, *ACS Sustainable Chemistry and Engineering* **2020**, *8*, 33.
[38] M. Wang, K. Liu, J. Yu, Q. Zhang, Y. Zhang, M. Valix, D. C. W. Tsang, *Global Challenges* **2023**, *7*, 3.
[39] Y. Ji, C. T. Jafvert, F. Zhao, *Resources, Conservation and Recycling* **2021**, *170*, 105551.
[40] B. Zhang, H. Xie, B. Lu, X. Chen, P. Xing, J. Qu, Q. Song, H. Yin, *ACS Sustainable Chemistry and Engineering* **2019**, *7*, 15.
[41] M. Mirza, R. Abdulaziz, W. C. Maskell, C. Tan, P. R. Shearing, D. J. L. Brett, *Electrochimica Acta* **2021**, *391*, 138846.
[42] S. He, A. Zhou, T. Jiang, Z. Liu, *Journal of Cleaner Production* **2023**, *422*, 138511.
[43] H. Zhang, H. Ning, J. Busbee, Z. Shen, C. Kiggins, Y. Hua, J. Eaves, J. Davis III, T. Shi, Y.-T. Shao, J.-M. Zuo, X. Hong, Y. Chan, S. Wang, P. Wang, P. Sun, S. Xu, J. Liu, P. V. Braun, *Science Advances* **2017**, *3*, 5.
[44] B. Zahiri, A. Patra, C. Kiggins, A. X. B. Yong, E. Ertekin, J. B. Cook, P. V. Braun, *Nature Materials* **2021**, *20*, 1392.
[45] A. Patra, J. Davis III, S. Pidaparthy, H. H. Karigerasi, B. Zahiri, A. A. Kulkarni, M. A. Caple, D. P. Shoemaker, J. M. Zuo, P. V. Braun, *PNAS* **2021**, *118*, 22.
[46] A. J. Bard, L. R. Faulkner, *Electrochemical Methods: Fundamentals and Applications*, 2nd edn, John Wiley & Sons, Incorporated, New York **2000**.
[47] T. F. Fuller, J. N. Harb, *Electrochemical Engineering*, John Wiley & Sons, Incorporated, New York **2018**.
[48] L. Li, J. Ge, F. Wu, R. Chen, S. Chen, B. Wu, *Journal of Hazardous Materials* **2010**, *176*, 1.
[49] J. Nan, D. Han, X. Zuo, *J. Power Sources* **2005**, *152*, 278.
[50] S. Sloop, L. Crandon, M. Allen, K. Koetje, L. Reed, L. Gaines, W. Sirisaksoontorn, M. Lerner, *Sustain. Mater.Technol.* **2020**, *25*, e00152.
[51] J. B. Dunn, C. James, L. Gaines, K. Gallagher, D. Qiang, J. C. Kelly, Material and energy flows in the production of cathode and anode materials for lithium ion batteries, No. ANL/ESD-14/10 Rev, Argonne National Laboratory, IL **2015**.
[52] M. Goedkoop, R. Heijungs, A. D. Schryver, J. Struijs, R. V. Zelm,Recipe 2008 a life cycle impact assessment method which comprises harmonised category indicators at the midpoint and the endpoint level, *Report I: Characterization*, Dutch Ministry of Housing, Spatial Planning and the Environment **2009**.
[53] Q. Dai, J. Spangenberger, S. Ahmed, L. Gaines, J. C. Kelly, M. Wang, Everbatt: A closed-loop battery recycling cost and environmental impacts model No. ANL-19/16, Argonne National Laboratory **2019**, https://publications.anl.gov/anlpubs/2019/07/153050.pdf (accessed: March 2025)